Inorganic Chemistry

Article

pubs.acs.org/IC

Valence Transitions in Negative Thermal Expansion Material $SrCu_3Fe_4O_{12}$

Ikuya Yamada,*[,†,‡] Kentaro Shiro,[§] Hidenobu Etani,[§] Shohei Marukawa,[∥] Naoaki Hayashi,[⊥] Masaichiro Mizumaki,[#,¶] Yoshihiro Kusano,[▽] Shigenori Ueda,[$] Hideki Abe,[‡,&] and Tetsuo Irifune[○]

[†]Nanoscience and Nanotechnology Research Center, Osaka Prefecture University, 1-2 Gakuen-cho, Naka-ku, Sakai, Osaka 599-8570, Japan

[‡]Precursory Research for Embryonic Science and Technology (PRESTO), Japan Science and Technology Agency (JST), Chiyoda-ku, Tokyo 102-0075, Japan

[§]Department of Chemistry, Graduate School of Science and Engineering, Ehime University, 2-5 Bunkyo-cho, Matsuyama, Ehime 790-8577, Japan

[∥]Department of Chemistry, Graduate School of Science, Osaka Prefecture University, 1-1 Gakuen-cho, Naka-ku, Sakai, Osaka 599-8531, Japan

[⊥]Institute for Integrated Cell-Material Sciences (iCeMS), Kyoto University, Yoshidaushinomiya-cho, Sakyo-ku, Kyoto 606-8501, Japan

[#]Japan Synchrotron Radiation Research Institute (JASRI), Sayo-cho, Sayo-gun, Hyogo 679-5198, Japan

[¶]Core Research for Evolutional Science and Technology (CREST), JST, 5 Sanbancho, Chiyoda-ku, Tokyo 102-0075, Japan

[▽]Department of Applied Arts and Design, Kurashiki University of Science and the Arts, Kurashiki, Okayama 712-8505, Japan

[$]Synchrotron X-ray Station at SPring-8, National Institute for Materials Science (NIMS), Sayo, Hyogo 679-5148, Japan

[&]Environmental Remediation Materials Center, NIMS, 1-1 Namiki, Tsukuba 305-0044, Japan

[○]Geodynamics Research Center (GRC), Ehime University, 2-5 Bunkyo-cho, Matsuyama, Ehime 790-8577, Japan

Supporting Information

ABSTRACT: The valence states of a negative thermal expansion material, $SrCu_3Fe_4O_{12}$, are investigated by X-ray absorption and ^{57}Fe Mössbauer spectroscopy. Spectroscopic analyses reveal that the appropriate ionic model of this compound at room temperature is $Sr^{2+}Cu^{\sim 2.4+}{}_3Fe^{\sim 3.7+}{}_4O_{12}$. The valence states continuously transform to $Sr^{2+}Cu^{\sim 2.8+}{}_3Fe^{\sim 3.4+}{}_4O_{12}$ upon cooling to ~200 K, followed by a charge disproportionation transition into the $Sr^{2+}Cu^{\sim 2.8+}{}_3Fe^{3+}{}_{\sim 3.2}Fe^{5+}{}_{\sim 0.8}O_{12}$ valence state at ~4 K. These observations have established the charge-transfer mechanism in this compound, and the electronic phase transitions in $SrCu_3Fe_4O_{12}$ can be distinguished from the first-order charge-transfer phase transitions ($3Cu^{2+} + 4Fe^{3.75+} \rightarrow 3Cu^{3+} + 4Fe^{3+}$) in $Ln^{3+}Cu^{2+}{}_3Fe^{3.75+}{}_4O_{12}$ (Ln = trivalent lanthanide ions).

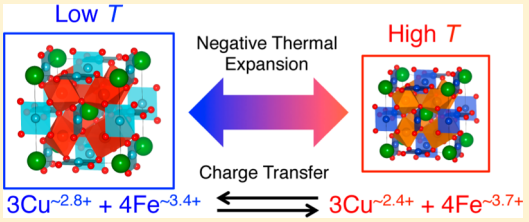

1. INTRODUCTION

Negative thermal expansion (NTE) materials are of interest in materials science and technologies because of their usefulness in the precise control of coefficients of thermal expansion (CTE).[1,2] Several mechanisms for NTE are currently proposed: magnetovolume effects, framework structures, ferroelectric phase transitions, and valence transitions (charge transfers). NTE materials induced by the former three mechanisms have been extensively studied in the past 2 decades. A cubic antiperovskite nitride $Mn_3(Cu,Ge)N$ shows a large NTE with a linear CTE of α_L = ca. -2×10^{-5} K^{-1} in the vicinity of room temperature.[3] The large NTE of this compound is achieved by broadening the magnetovolume effect (Invar effect) of the parent Mn_3AN compounds (A = Ni, Zn, Ga)[4] with chemical substitutions. ZrW_2O_8 shows a NTE because of its framework structure in a wide temperature range of 2−1000 K, in which transverse atomic vibrations in the Zr−O−W linkages generate shrinkage of the Zr−W distances upon heating, leading to volume expansion.[5] A perovskite oxide, $PbTiO_3$, displays a ferroelectric phase transition with an abrupt volume change at ~760 K, followed by a NTE with a volumetric CTE of α_V = ca. -2×10^{-6} K^{-1} between 300 and 760 K.[6] Chemical substitutions on this compound also achieve broadening of the first-order phase transition, resulting in enhanced NTE with wider temperature windows (e.g., α_V = ca. -3.92×10^{-5} K^{-1} in 298−923 K).[7]

Valence-transition-induced NTE is proposed in rare-earth fulleride. $Sm_{2.75}C_{60}$ shows a NTE with $\alpha_V = -3 \times 10^{-5}$ K^{-1} between 4.2 and 32 K.[8] Although the Sm valence transition

Received: July 11, 2014
Published: September 11, 2014

   dx.doi.org/10.1021/ic501665c | Inorg. Chem. 2014, 53, 10563−10569

between +(2 + δ) and +2 in the NTE temperature range is suggested, spectroscopic investigation confirms that the Sm valence was unchanged during NTE.[9] A perovskite oxide, (Bi,La)NiO_3, was recently reported as a colossal NTE material with $\alpha_L = -8.2 \times 10^{-5}$ K^{-1}.[10] A significant volume expansion (~2.6%) is induced in the pure $BiNiO_3$ compound by a first-order phase transition ($Bi^{3+}Ni^{3+}O_3 \rightarrow Bi^{3+}_{1/2}Bi^{5+}_{1/2}Ni^{2+}O_3$). The Ni−O bonds are elongated by the valence transition from Ni^{3+} to Ni^{2+},[11] which is evidenced by soft X-ray absorption spectroscopy of Ni K-edge.[12] The temperature range where the high-temperature small-volume and low-temperature large-volume phases coexist is expanded by chemical substitution, resulting in NTE-like behaviors in the bulk forms of (Bi,Ln)NiO_3 (Ln = trivalent lanthanide ions).[10,13,14]

The cubic $AA'_3B_4O_{12}$-type complex perovskite oxide $SrCu_3Fe_4O_{12}$ shows a NTE within a temperature range of 170−270 K with $\alpha_L = -2.3 \times 10^{-5}$ K^{-1}.[15] In this compound, Cu ions at A′ sites and Fe ions at B sites are coordinated by four and six O ions to form CuO_4 pseudosquares and FeO_6 octahedra, respectively, as shown in Figure 1.[16] The electronic

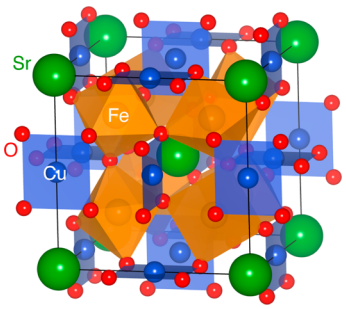

Figure 1. Crystal structure of $SrCu_3Fe_4O_{12}$ drawn using *VESTA* software.[16] The large (green) and small (red) spheres represent Sr and O ions, respectively. The squares and octahedra indicate CuO_4 and FeO_6 polyhedral units, respectively.

interactions between the Cu and Fe ions dominate the anomalous structural and electronic properties of this material. Crystal structure analysis and Mössbauer spectroscopy propose that NTE of this compound is associated with an intersite charge transfer between the Cu and Fe ions ($Cu^{2+} + Fe^{4+} \rightarrow Cu^{3+} + Fe^{3+}$ in a simple representation) and the resulting continuous Fe−O bond elongation upon cooling.[15] NTE in $SrCu_3Fe_4O_{12}$ is a second-order type, and the thermal hysteresis is negligibly small,[17] both of which are advantageous in practical applications. NTE in $SrCu_3Fe_4O_{12}$ is distinguishable from the abrupt volume changes induced by first-order intersite charge-transfer transitions ($3Cu^{2+} + 4Fe^{3.75+} \rightarrow 3Cu^{3+} + 4Fe^{3+}$) in analogue $A^{3+}Cu_3Fe_4O_{12}$ compounds (A = La, Pr, Nd, Sm, Eu, Gd, Tb, Bi) and the charge disproportionation transition ($2Fe^{4+} \rightarrow Fe^{3+} + Fe^{5+}$) for $Ca^{2+}Cu^{2+}{}_3Fe^{4+}{}_4O_{12}$.[18−21] The electronic states of this system are derived from the ligand hole character of the unusually high valence ions of Fe^{4+} ($d^5\underline{L}^1$ electron configuration; $\underline{L}$ represents an oxygen ligand hole) and Cu^{3+} ($d^9\underline{L}^1$).[22−24] Thus, the charge-transfer transitions in $A^{3+}Cu_3Fe_4O_{12}$ are represented as $3d^9 + 4d^5\underline{L}^{0.75} \rightarrow 3d^9\underline{L}^1 + 4d^5$. Careful investigations of the electronic states are necessary for elucidating the valence transition mechanism for NTE of $SrCu_3Fe_4O_{12}$. However, until now, the charge-transfer transformation in $SrCu_3Fe_4O_{12}$ has been proposed only based on crystal structure refinement and ^{57}Fe Mössbauer spectroscopy,[15] and the detailed valence transition processes have not been illustrated.

In this paper, we report the spectroscopic investigation of the Cu and Fe ions in $SrCu_3Fe_4O_{12}$. The X-ray absorption near-edge structure (XANES) of the Cu K-edge and soft X-ray absorption spectrometry (XAS) spectrum of the Cu L_3-edge indicate a continuous valence transition of the Cu ions from ~2.4 to ~2.8 upon cooling from room temperature to below ~200 K. Correspondingly, Mössbauer spectroscopy analyses reveal the valence transition of the Fe ions, from ~3.7 at room temperature to ~3.4 at 4 K. The overall spectroscopic analyses elucidate the anomalous noninteger valence states of the Cu and Fe ions and charge-transfer processes in $SrCu_3Fe_4O_{12}$.

2. EXPERIMENTAL SECTION

The same $LnCu_3Fe_4O_{12}$ (Ln = La, Pr, Nd, Sm, Eu) samples as those in ref 20 were adopted for synchrotron powder X-ray diffraction (SXRD) and XANES measurements. A polycrystalline sample of $SrCu_3Fe_4O_{12}$ for SXRD, XAS, XANES, and Mössbauer spectroscopy measurements was prepared under high-pressure and high-temperature conditions of 20 GPa and 1473 K, respectively. The high-pressure and high-temperature treatments were performed using a Kawai-type high-pressure apparatus, as described in previous reports.[25] X-ray diffraction (XRD) measurements were conducted at temperatures between 100 and 450 K using a Rigaku Ultima IV X-ray diffractometer with Cu Kα radiation. SXRD measurements of $SrCu_3Fe_4O_{12}$ and $LnCu_3Fe_4O_{12}$ (Ln = La, Pr, Nd, Sm, Eu) were conducted at temperatures between 100 and 450 K at the BL02B2 beamline of SPring-8. The powder samples were charged into Lindemann glass capillary tubes of 0.2 mm inner diameter. The wavelengths used in the SXRD measurements were 0.42023 and 0.42085 Å for $SrCu_3Fe_4O_{12}$ and $LnCu_3Fe_4O_{12}$, respectively, and were determined using a CeO_2 standard. Lattice constants and structural parameters were refined based on the XRD and SXRD data, respectively, using the program *RIETAN-FP*.[26] Electron diffraction (ED) patterns of $SrCu_3Fe_4O_{12}$ were collected at 108 and 296 K using a JEOL JEM-2100F transmission electron microscope with an accelerating voltage of 200 kV.

Cu K-edge XANES data for $SrCu_3Fe_4O_{12}$ and $LnCu_3Fe_4O_{12}$ (Ln = La, Pr, Nd, Sm, Eu) were collected in a temperature range between 8 and 300 K at the BL01B1 beamline of SPring-8. XAS measurements of the Cu L_3-edge for $SrCu_3Fe_4O_{12}$ were conducted between 12 and 300 K using a total electron yield method at the BL27SU beamline of SPring-8. ^{57}Fe Mössbauer spectra of $SrCu_3Fe_4O_{12}$ were collected between 4 and 400 K in transmission geometry mode using ^{57}Co/Rh as a radiation source and α-Fe as a control for velocity calibration and isomer shift (IS). The collected Mössbauer spectra were fitted computationally using the Lorentzian function. Hard X-ray photoemission spectroscopy (HAXPES) data of the valence band of $SrCu_3Fe_4O_{12}$ were collected at temperatures between 20 and 300 K using a high-resolution hemispherical electron analyzer (VG SCIENTA R4000) installed at the undulator beamline BL15XU[27,28] of SPring-8. The incident photon energy was set to 5.95 keV. The total energy resolution was 235 meV, which was confirmed by the Fermi cutoff of an evaporated Au film. The binding energy was referred to the Fermi level of the Au film. The electrical resistivity of the sintered polycrystalline sample of $SrCu_3Fe_4O_{12}$ was measured by the standard four-probe method using a Quantum Design Physical Properties Measurement System.

3. RESULTS AND DISCUSSION

The good quality of the $SrCu_3Fe_4O_{12}$ sample was confirmed by the SXRD data, which resulted in satisfactory crystal structure refinement (see Figure S1 and Table S1 in the Supporting Information, SI). Although small amounts of impurity phases (CuO and unknown phases of presumably less than a few percent) were detected, the quality of the sample was better than those reported in previous studies.[15,17] This is because the

dx.doi.org/10.1021/ic501665c | Inorg. Chem. 2014, 53, 10563−10569

synthesis pressure in this study (20 GPa) was higher than those used previously (15 GPa), which is the same trend as that observed in the synthesis of the Ca analogue.[21] The decrease in the fraction of Fe-containing impurity phases improved the Mössbauer spectroscopy data, as shown later, contributing to the precise determination of the Fe valence states.

Figure 2 shows the ED patterns of $SrCu_3Fe_4O_{12}$ along the $[1\bar{1}0]$ zone axis at 108 and 296 K. No additional reflection

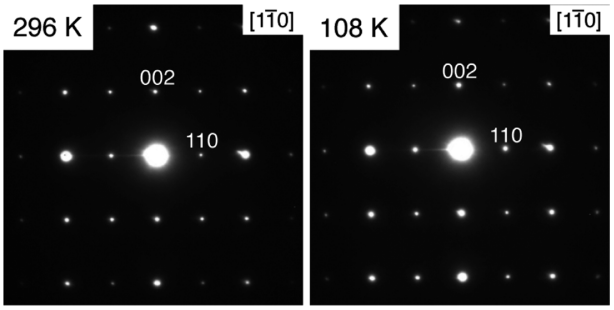

Figure 2. ED patterns of $SrCu_3Fe_4O_{12}$ along the $[1\bar{1}0]$ zone axis collected at 108 and 296 K.

spots appeared upon cooling. Thus, the ED patterns could be indexed with the space group of $Im\bar{3}$ (No. 204) at these temperatures, confirming the absence of charge ordering for $SrCu_3Fe_4O_{12}$, unlike the charge-disproportionated phase of $CaCu_3Fe_4O_{12}$, in which rock-salt-type charge ordering of Fe^{3+} and Fe^{5+} ions is predominant.[21] This is because of the large deviation from the ideal abundance ratio of Fe^{3+}:Fe^{5+} for the rock-salt-type ordering (=1:1) in the low-temperature charge-disproportiontaed $SrCu_3Fe_4O_{12}$ phase, as shown in the Mössbauer spectroscopy later. Thus, we made crystal structure refinement of $SrCu_3Fe_4O_{12}$ based on the space group $Im\bar{3}$ over the entire temperature range between 100 and 450 K. Figure 3 shows the temperature dependence of the unit cell volumes normalized at 450 K, and the Cu−O and Fe−O bond lengths obtained from the SXRD Rietveld refinement results for $LnCu_3Fe_4O_{12}$ (Ln = La, Pr, Nd, Sm, Eu) and $SrCu_3Fe_4O_{12}$, in which part of the data are adopted from a previous report.[20] Abrupt volume expansions associated with first-order charge-transfer transitions are confirmed at temperatures between 240 and 360 K for $LnCu_3Fe_4O_{12}$.[20] The volume expansion rates for $LnCu_3Fe_4O_{12}$ have a range of ∼1.4% (Ln = La) to ∼2.0% (Ln = Eu). In contrast, $SrCu_3Fe_4O_{12}$ displays a continuous volume expansion from 280 to 180 K upon cooling, which is consistent with a previous report.[15] Note that the volume expansion rate for $SrCu_3Fe_4O_{12}$ (∼0.3%) is much smaller than that for $LnCu_3Fe_4O_{12}$. In addition, we confirm the differences in the shrinkage/elongation rates of the metal−oxygen bonds between $LnCu_3Fe_4O_{12}$ and $SrCu_3Fe_4O_{12}$. The Cu−O and Fe−O bonds respectively change by approximately −0.045 and +0.033 Å at the phase transition temperatures of $LnCu_3Fe_4O_{12}$ and by approximately −0.019 and +0.008 Å in the NTE temperature range for $SrCu_3Fe_4O_{12}$ (see Figure 3), implying that the amount of charge transfer in $SrCu_3Fe_4O_{12}$ is much smaller than those in $LnCu_3Fe_4O_{12}$.

The valence states of $SrCu_3Fe_4O_{12}$ were investigated by multiple spectroscopic techniques. Figure 4 shows Cu K-edge XANES spectra for $LnCu_3Fe_4O_{12}$ (Ln = La, Pr, Nd, Sm, Eu) and $SrCu_3Fe_4O_{12}$. $LnCu_3Fe_4O_{12}$ (Ln = Nd, Sm, Eu) have valence states identical with those of $Ln^{3+}Cu^{2+}{}_3Fe^{3.75+}{}_4O_{12}$ at room temperature as reported previously.[20] The XANES

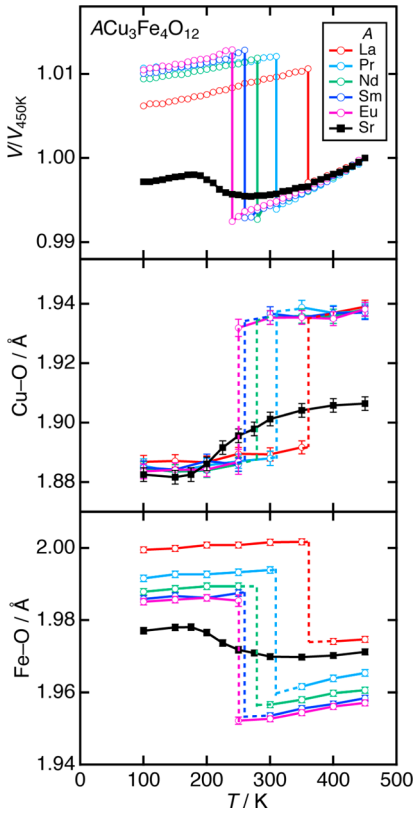

Figure 3. Temperature dependence of the normalized unit cell volume and the Cu−O and Fe−O bond lengths for $SrCu_3Fe_4O_{12}$ and $LnCu_3Fe_4O_{12}$ (Ln = La, Pr, Nd, Sm, Eu). The unit cell volumes between 100 and 450 K and bond lengths at 100 and 450 K for $LnCu_3Fe_4O_{12}$ were adopted from ref 12.

spectra of these compounds consist of a preedge peak (P) attributed to 1s → 3d transition and four absorption peaks (A−D) derived from 1s → 4p transitions. Peak B (D) corresponds to the 1s → 4pπ (1s → 4pσ) transition and peak A (C) its shakedown. The appearance of sharp shakedown peak A is characteristic of XANES spectra of Cu^{2+} oxides with square-planar coordination.[29] The room temperature XANES spectrum of $LaCu_3Fe_4O_{12}$ shows a significant shift of ∼2 eV toward higher energy (see the inset of Figure 4a) compared with those of $LnCu_3Fe_4O_{12}$ (Ln = Nd, Sm, Eu), because trivalent Cu ions are predominant in the $La^{3+}Cu^{3+}{}_3Fe^{3+}{}_4O_{12}$ phase at room temperature.[18] The XANES spectrum of $PrCu_3Fe_4O_{12}$ exhibits an intermediate shape between those for Cu^{2+} and Cu^{3+} spectra because the $Pr^{3+}Cu^{2+}{}_3Fe^{3.75+}{}_4O_{12}$ and $Pr^{3+}Cu^{3+}{}_3Fe^{3+}{}_4O_{12}$ phases coexist at room temperature.[20] Figure 4b shows the evolution of the XANES spectrum of $EuCu_3Fe_4O_{12}$ with temperature. The valence transition in Cu ions (Cu^{2+} → Cu^{3+}) is clearly observed as ∼2 eV shifts from 260 and 240 K to higher energy. The above results allow us to confirm that the Cu K-edge XANES spectra consistently reflect the Cu valences for $LnCu_3Fe_4O_{12}$. It is reported that differences in the Cu valence can be distinguished in XANES spectra from a number of particular features.[30] One is the position of the preedge peak. The preedge peak shifts by ca. 2 eV from Cu^{2+} to Cu^{3+} in the same coordination environment. Another is a separation between peaks A and B. Because the positions of peaks B and D shift significantly compared with their shakedown peaks A and C in the valence transition from Cu^{2+} to Cu^{3+}, the separation between peaks A and B apparently

dx.doi.org/10.1021/ic501665c | Inorg. Chem. 2014, 53, 10563−10569

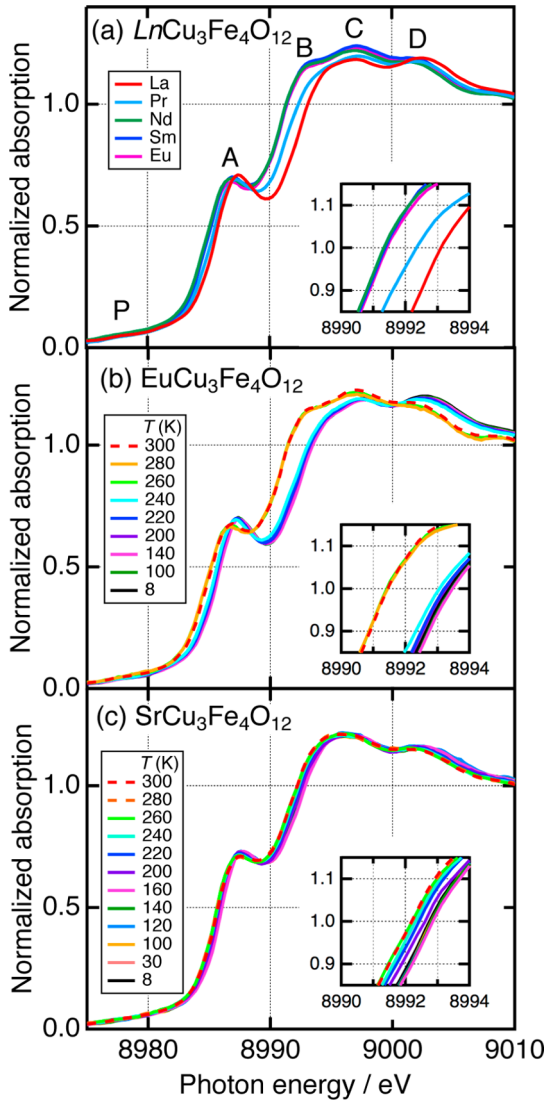

Figure 4. (a) Cu K-edge XANES spectra of $LnCu_3Fe_4O_{12}$ (Ln = La, Pr, Nd, Sm, Eu) collected at room temperature. Temperature evolution of Cu K-edge XANES spectra for (b) $EuCu_3Fe_4O_{12}$ and (c) $SrCu_3Fe_4O_{12}$. The insets show the enlarged spectra in the vicinity of the absorption edge.

increases. For $SrCu_3Fe_4O_{12}$ and $LnCu_3Fe_4O_{12}$, the preedge peaks are too weak to evaluate their shifts precisely. In contrast, significant shifts of the standard absorption edge energy (E_0), in which the normalized absorption is unity, arise from the increase in the separation between peaks A and B (see the insets of Figure 4a,b). E_0 retains almost the same value (~8991.3 eV) for the Cu^{2+} ions of $LnCu_3Fe_4O_{12}$ (Ln = Nd, Sm at room temperature and Ln = Eu at 260, 280, and 300 K) but becomes 8993.1−8993.5 eV for the Cu^{3+} ions of $LnCu_3Fe_4O_{12}$ (Ln = La at room temperature and Ln = Eu at below 240 K). The clear gap (~2 eV) between the E_0 values of the Cu^{2+} and Cu^{3+} valence states allows us to estimate Cu valences from E_0, as shown later.

Figure 4c shows Cu K-edge XANES spectra for $SrCu_3Fe_4O_{12}$. The spectral shapes are similar to those of $LnCu_3Fe_4O_{12}$. E_0 gradually shifts from 8992.2 to 8992.9 eV upon cooling from 260 to 150 K, indicating an increase in the Cu valence. Note that the E_0 range of $SrCu_3Fe_4O_{12}$ is confined to that of $LnCu_3Fe_4O_{12}$ (8991.3−8993.5 eV). This means that the Cu valence of $SrCu_3Fe_4O_{12}$ changes within noninteger numbers between +2 and +3, in contrast to the Cu valence transitions between integer numbers for $LnCu_3Fe_4O_{12}$.

The noninteger valences and valence transitions of the Cu ions in $SrCu_3Fe_4O_{12}$ are also confirmed by the Cu L_3-edge XAS results. Figure 5 shows Cu L_3-edge XAS spectra of $SrCu_3Fe_4O_{12}$

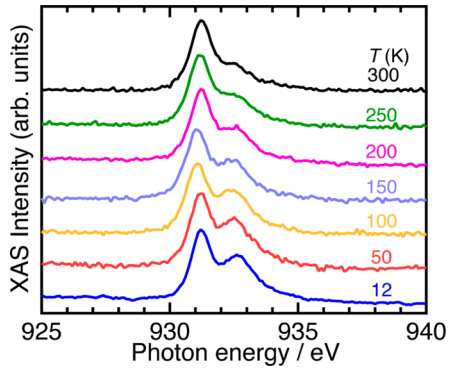

Figure 5. Cu L_3-edge XAS of $SrCu_3Fe_4O_{12}$ at temperatures of 12−300 K.

collected at temperatures between 12 and 300 K. The main peaks at ~931 eV are attributed to white lines arising from $2p^63d^9 \rightarrow 2p^53d^{10}$ transformation and are typical for Cu^{2+} ions, whereas the shoulder peaks at ~932.5 eV are predominant in Cu^{3+} oxides.[31,32] The $Ln^{3+}Cu^{2+}{}_3Fe^{3.75+}{}_4O_{12}$ phases do not have shoulder peaks,[20] indicating that the Cu valences are purely 2+. Conversely, the existence of the shoulder peak for $SrCu_3Fe_4O_{12}$ at room temperature is interpreted as an intermediate valence such as $Cu^{(2+\delta)+}$. The shoulder peak is gradually enhanced upon cooling. The temperature evolution of the shoulder peak intensity is considered to arise from the increase in the Cu valence. These experimental results lead us to safely conclude that intermediate valence states are predominant for Cu ions in $SrCu_3Fe_4O_{12}$ within the measured temperature range.

Next, we evaluate the valence transformation of Cu ions for $SrCu_3Fe_4O_{12}$. Figure 6a shows the temperature dependence of E_0 for $EuCu_3Fe_4O_{12}$ and $SrCu_3Fe_4O_{12}$. A discontinuous change in E_0 occurs between 240 and 260 K for $EuCu_3Fe_4O_{12}$, corresponding to the Cu valence transition attributed to the intersite charge transfer ($3Cu^{2+} + 4Fe^{3.75+} \rightarrow 3Cu^{3+} + 4Fe^{3+}$), as reported previously.[20] A slight increase in E_0 upon cooling from 240 to 150 K derives from the fact that the $Eu^{3+}Cu^{2+}{}_3Fe^{3.75+}{}_4O_{12}$ and $Eu^{3+}Cu^{3+}{}_3Fe^{3+}{}_4O_{12}$ phases coexist and the phase fraction gradually changes (see the XRD data in ref 20). E_0 gradually increases upon cooling from 260 to 160 K for $SrCu_3Fe_4O_{12}$, while no notable changes are observed in other temperature ranges. This indicates a gradual increase in the Cu valence induced by the continuous charge transfer. Figure 6b shows estimated Cu valences as a function of E_0 for $SrCu_3Fe_4O_{12}$ and $EuCu_3Fe_4O_{12}$. We assume a linear relationship between E_0 and the Cu valence in which E_0 values at 8 and 300 K for $EuCu_3Fe_4O_{12}$ correspond to Cu^{3+} and Cu^{2+}, respectively. The E_0 data for $SrCu_3Fe_4O_{12}$ are plotted on the analytical curve obtained from the above assumption. These plots show that the Cu valence of $SrCu_3Fe_4O_{12}$ continuously changes from ~2.4 (260−300 K) to ~2.8 (8−160 K).

Figure 7 shows Mössbauer spectra for $SrCu_3Fe_4O_{12}$. At temperatures above 210 K, a primary singlet (Fe ions occupying B sites) and a small amount of doublet (Fe ions incorporated into the A′ site) components are observed (see

dx.doi.org/10.1021/ic501665c | Inorg. Chem. 2014, 53, 10563−10569

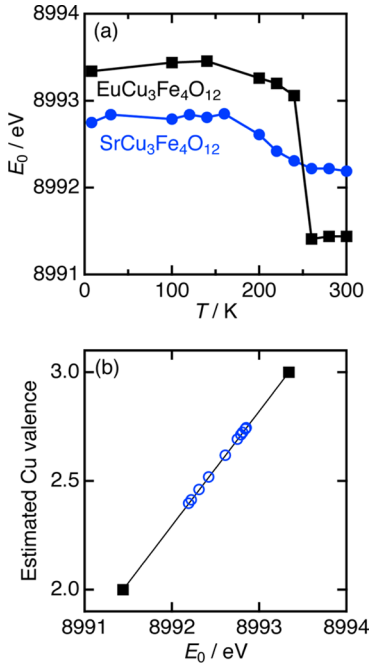

Figure 6. (a) Temperature dependence of the Cu K-edge X-ray absorption edge energy (E_0) for $SrCu_3Fe_4O_{12}$ and $EuCu_3Fe_4O_{12}$. (b) Cu K-edge absorption edge energy versus estimated Cu valence for $SrCu_3Fe_4O_{12}$. The squares represent E_0 of $EuCu_3Fe_4O_{12}$ at 8 and 300 K, and the line represents the analytical curve. The circles represent $SrCu_3Fe_4O_{12}$ data plotted on the analytical curve.

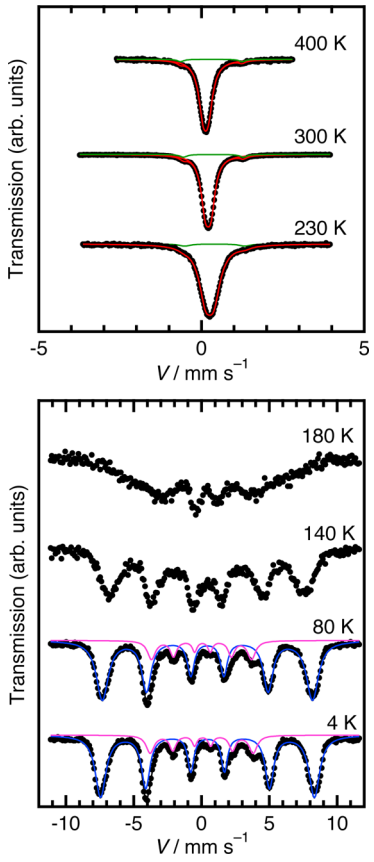

Figure 7. Mössbauer spectra of $SrCu_3Fe_4O_{12}$ at temperatures between 4 and 400 K. The circles represent the observed data. The lines represent fitting results for the following components: red (B site), green (A′ site), blue (Fe^{3+}), purple (Fe^{5+}), and black (total).

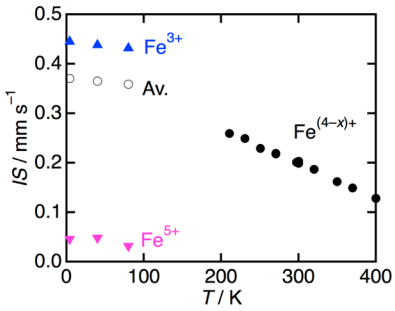

Figure 8. Temperature dependence of the IS value for $SrCu_3Fe_4O_{12}$.

the hyperfine parameters listed in Table S2 in the SI). The singlet component splits into two sextets, attributed to Fe^{3+} and Fe^{5+} ions, below ~200 K, as observed in a previous report.[15] Components derived from small amounts of impurity phases were not observed in this study because of the good quality of the sample, as shown by the SXRD data. The abundance ratio at 4 K is Fe^{3+}:Fe^{5+} = 82:18, resulting in an averaged Fe valence of +3.36. Unfortunately, the significant broadening of the spectra in the intermediate temperature range (~100−200 K) disturbs reliable fitting of the spectra. Figure 8 shows the temperature dependence of the IS of $SrCu_3Fe_4O_{12}$. We confirm a monotonic change in the IS value within the measured temperature range. In the upper half of the NTE temperature range (~210−280 K), the continuous decrease in IS upon heating appears to be within a conventional temperature-dependent second-order Doppler shift. This is because the magnitude of the Fe valence change is too small to detect by Mössbauer spectroscopy.

We conducted comprehensive analysis of the valence states of the Cu and Fe ions in $SrCu_3Fe_4O_{12}$ by combining the Cu K-edge X-ray absorption and ^{57}Fe Mössbauer spectroscopy data. The IS value at room temperature (0.20 mm s^{-1}) is slightly larger than those (0.16−0.18 mm s^{-1}) of the $A^{3+}Cu^{2+}{}_3Fe^{3.75+}{}_4O_{12}$ phases (A = Eu, Tb, Dy, Lu, Y),[20,25] indicating that the formal Fe valence of $SrCu_3Fe_4O_{12}$ is not pure +4 but close to or even lower than +3.75. The Cu valence estimated from the Cu K-edge XANES data results in a calculated Fe valence for ~3.7 at room temperature based on the charge neutrality, supporting the Mössbauer spectroscopy analysis results. Thus, the appropriate ionic model at room temperature can be represented as $Sr^{2+}Cu^{\sim 2.4+}{}_3Fe^{\sim 3.7+}{}_4O_{12}$. For the charge-disproportionated $SrCu_3Fe_4O_{12}$ phase at low temperature, Fe (~3.36) and Cu (~2.8) valence states were respectively estimated from the Mössbauer and XANES analyses as shown above. These valence states reasonably compensate for the charge neutrality. Considering the above, the temperature evolution of the valence states for $SrCu_3Fe_4O_{12}$ can be interpreted as follows: $Sr^{2+}Cu^{\sim 2.4+}{}_3Fe^{\sim 3.7+}{}_4O_{12}$ (~300 K) → $Sr^{2+}Cu^{\sim 2.8+}{}_3Fe^{\sim 3.4+}{}_4O_{12}$ (~200 K) → $Sr^{2+}Cu^{\sim 2.8+}{}_3Fe^{3+}{}_{\sim 3.2}Fe^{5+}{}_{\sim 0.8}O_{12}$ (~4 K). The degree of Fe valence transition during the intersite charge transfer is calculated to be ~0.3 per Fe ion for $SrCu_3Fe_4O_{12}$, which is only 40% of that (=0.75) for $LnCu_3Fe_4O_{12}$. This reasonably explains the smaller rate of unit cell volume change in NTE of $SrCu_3Fe_4O_{12}$ than those for the first-order phase transitions of $LnCu_3Fe_4O_{12}$, as guessed earlier. To our knowledge, this is the first direct observation of the continuous valence transitions associated with NTE.

dx.doi.org/10.1021/ic501665c | Inorg. Chem. 2014, 53, 10563−10569

Figure 9 shows the electrical resistivity of $SrCu_3Fe_4O_{12}$, together with that of $CaCu_3Fe_4O_{12}$.[21] Semiconductor-like

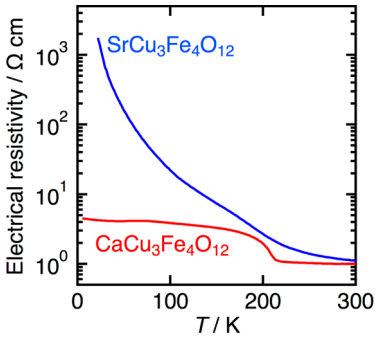

Figure 9. Temperature dependence of the electrical resistivity for $ACu_3Fe_4O_{12}$ (A = Ca, Sr). The data for $CaCu_3Fe_4O_{12}$ were taken from ref 21.

character was predominant for $SrCu_3Fe_4O_{12}$ down to the lowest temperature (~20 K). This is in stark contrast to the metal-to-semiconductor transition of $CaCu_3Fe_4O_{12}$ at the charge disproportionation transition temperature of 210 K.[21] The intrinsic electrical transport property of $SrCu_3Fe_4O_{12}$ was difficult to observe probably because the grain boundary conduction effect was not negligible. Figure 10 shows the

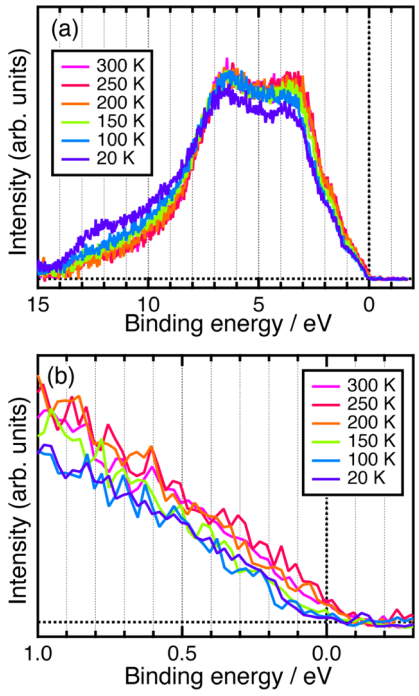

Figure 10. (a) HAXPES spectra of the valence band between 20 and 300 K for $SrCu_3Fe_4O_{12}$. (b) Enlarged spectra in the vicinity of Fermi energy.

valence-band HAXPES spectra of $SrCu_3Fe_4O_{12}$. The whole spectral weight gradually shifted to deeper energy level, and the density of states in the vicinity of Fermi energy decreased below 200 K. This confirms that the electrical conductivity decreases with charge disproportionation, although the charge-transfer transition hardly affected the electrical conductivity. Careful investigations using a single crystal and theoretical calculation are needed to unveil the electrical transport property of $SrCu_3Fe_4O_{12}$, but it is beyond the present study.

The above analyses demonstrate the unusual valence states of $SrCu_3Fe_4O_{12}$. In general, $A^{2+}Cu^{2+}{}_3B^{4+}{}_4O_{12}$ valence states are dominant in isostructural compounds although slight deviations from integer oxidation numbers are recognized in transition-metal ions such as Cu^{2+}, V^{4+}, and Ru^{4+}.[33−35] Surprisingly, the Fe valence in the high-temperature phase of $SrCu_3Fe_4O_{12}$ is comparable to or even lower than that in the electron-doped $A^{3+}Cu^{2+}{}_3Fe^{3.75+}{}_4O_{12}$ phases. In the ligand hole picture, ligand holes exist at both hybridized Cu 3d−O 2p and Fe 3d−O 2p bands in $SrCu_3Fe_4O_{12}$, although the ligand holes exist at either the Cu 3d−O 2p (as Cu^{3+}, $3d^9\underline{L}^1$ configuration[24]) or Fe 3d−O 2p (as $Fe^{3.75+}$, $3d^5\underline{L}^{0.75}$ configuration[22,23]) band in any electronic phases of $A^{3+}Cu_3Fe_4O_{12}$. This suggests that the energy levels of the Cu and Fe 3d bands are very close for $SrCu_3Fe_4O_{12}$ and/or the covalencies of the Cu−O and Fe−O bonds are strong enough to promote charge transfer between Cu and Fe ions in a wide temperature range. As a result, charge transfer (or ligand hole transfer) with NTE occurs gradually in $SrCu_3Fe_4O_{12}$. This is also different from relaxation of the first-order phase transitions by chemical substitution in NTE materials with other mechanisms. The fact that $SrCu_3Fe_4O_{12}$ displays NTE in a pure form, not solid solutions, enables us to develop novel NTE materials with a valence-transition mechanism based in a simpler design.

4. CONCLUSIONS

We have investigated the valence states and transformations of $SrCu_3Fe_4O_{12}$ using X-ray absorption and Mössbauer spectroscopy. The appropriate ionic model at room temperature is $Sr^{2+}Cu^{\sim 2.4+}{}_3Fe^{\sim 3.7+}{}_4O_{12}$. Unlike the first-order phase transitions in $ACu_3Fe_4O_{12}$ (A = La, Pr, Nd, Sm, Eu, Gd, Tb, Bi), an incomplete charge transfer between Cu and Fe ions arises continuously in the NTE temperature range, resulting in the $Cu^{\sim 2.8+}$ and $Fe^{\sim 3.4+}$ (or $Fe^{3+}{}_{\sim 4/5}Fe^{5+}{}_{\sim 1/5}$) valence states. These features illustrate the remarkable electronic state transformations in the copper−iron oxide system.

■ ASSOCIATED CONTENT

Supporting Information

SXRD and Rietveld refinement results, structure parameters, crystallographic data (CIF), and hyperfine parameters obtained from Mössbauer spectroscopy. This material is available free of charge via the Internet at http://pubs.acs.org.

■ AUTHOR INFORMATION

Corresponding Author

*E-mail: i-yamada@21c.osakafu-u.ac.jp.

Notes

The authors declare no competing financial interest.

■ ACKNOWLEDGMENTS

The authors thank K. Fujita, Y. Kususe, Y. Nakatsuka, T. Sato, T. Kuge, and Y. Daido for their support in XANES and XAS measurements. This work was carried out under the Visiting Researcher's Program of Geodynamics Research Center, Ehime University. The synchrotron radiation experiments were performed at SPring-8 with the approval of JASRI (Proposals 2012B1986, 2013A1042, 2013A1188, 2013A1689, 2013A1691, 2013B1063, and 2014A1206) and NIMS Synchrotron X-ray Station (Proposals 2013A4600 and 2013B4905). The authors

are grateful to HiSOR, Hiroshima University, and JAEA/SPring-8 for the development of HAXPES at BL15XU of SPring-8. This work was partially supported by the Murata Science Foundation and Nanotechnology Platform (Project 12024046) of the Ministry of Education, Culture, Sports, Science and Technology, Japan.

REFERENCES

(1) Evans, J. S. O. *J. Chem. Soc., Dalton Trans.* **1999**, 3317−3326.
(2) Takenaka, K. *Sci. Technol. Adv. Mater.* **2012**, *13*, 013001.
(3) Takenaka, K.; Takagi, H. *Appl. Phys. Lett.* **2005**, *87*, 261902.
(4) Fruchart, D.; Bertaut, E. F. *J. Phys. Soc. Jpn.* **1978**, *44*, 781−791.
(5) Mary, T. A.; Evans, J. S. O.; Vogt, T.; Sleight, A. W. *Science* **1996**, *272*, 90−92.
(6) Rossetti, G. A.; Cline, J. P.; Navrotsky, A. *J. Mater. Res.* **1998**, *13*, 3197−3206.
(7) Chen, J.; Xing, X. R.; Liu, G. R.; Li, J. H.; Liu, Y. T. *Appl. Phys. Lett.* **2006**, *89*, 101914.
(8) Arvanitidis, J.; Papagelis, K.; Margadonna, S.; Prassides, K.; Fitch, A. N. *Nature* **2003**, *425*, 599−602.
(9) He, S.; Nakatake, M.; Arita, M.; Cui, X.; Qiao, S.; Namatame, H.; Taniguchi, M.; Li, H. *Appl. Phys. Lett.* **2007**, *91*, 143103.
(10) Azuma, M.; Chen, W. T.; Seki, H.; Czapski, M.; Olga, S.; Oka, K.; Mizumaki, M.; Watanuki, T.; Ishimatsu, N.; Kawamura, N.; Ishiwata, S.; Tucker, M. G.; Shimakawa, Y.; Attfield, J. P. *Nat. Commun.* **2011**, *2*, 347.
(11) Ishiwata, S.; Azuma, M.; Hanawa, M.; Moritomo, Y.; Ohishi, Y.; Kato, K.; Takata, M.; Nishibori, E.; Sakata, M.; Terasaki, I.; Takano, M. *Phys. Rev. B* **2005**, *72*, 045104.
(12) Mizumaki, M.; Ishimatsu, N.; Kawamura, N.; Azuma, M.; Shimakawa, Y.; Takano, M.; Uozumi, T. *Phys. Rev. B* **2009**, *80*, 233104.
(13) Oka, K.; Mizumaki, M.; Sakaguchi, C.; Sinclair, A.; Ritter, C.; Attfield, J. P.; Azuma, M. *Phys. Rev. B* **2013**, *88*, 014112.
(14) Oka, K.; Nabetani, K.; Sakaguchi, C.; Seki, H.; Czapski, M.; Shimakawa, Y.; Azuma, M. *Appl. Phys. Lett.* **2013**, *103*, 061909.
(15) Yamada, I.; Tsuchida, K.; Ohgushi, K.; Hayashi, N.; Kim, J.; Tsuji, N.; Takahashi, R.; Matsushita, M.; Nishiyama, N.; Inoue, T.; Irifune, T.; Kato, K.; Takata, M.; Takano, M. *Angew. Chem., Int. Ed.* **2011**, *50*, 6579−6582.
(16) Momma, K.; Izumi, F. *J. Appl. Crystallogr.* **2011**, *44*, 1272−1276.
(17) Yamada, I.; Shiro, K.; Oka, K.; Azuma, M.; Irifune, T. *J. Ceram. Soc. Jpn.* **2013**, *121*, 912−914.
(18) Long, Y. W.; Hayashi, N.; Saito, T.; Azuma, M.; Muranaka, S.; Shimakawa, Y. *Nature* **2009**, *458*, 60−63.
(19) Long, Y. W.; Saito, T.; Tohyama, T.; Oka, K.; Azuma, M.; Shimakawa, Y. *Inorg. Chem.* **2009**, *48*, 8489−8492.
(20) Yamada, I.; Etani, H.; Tsuchida, K.; Marukawa, S.; Hayashi, N.; Kawakami, T.; Mizumaki, M.; Ohgushi, K.; Kusano, Y.; Kim, J.; Tsuji, N.; Takahashi, R.; Nishiyama, N.; Inoue, T.; Irifune, T.; Takano, M. *Inorg. Chem.* **2013**, *52*, 13751−13761.
(21) Yamada, I.; Takata, K.; Hayashi, N.; Shinohara, S.; Azuma, M.; Mori, S.; Muranaka, S.; Shimakawa, Y.; Takano, M. *Angew. Chem., Int. Ed.* **2008**, *47*, 7032−7035.
(22) Bocquet, A. E.; Mizokawa, T.; Saitoh, T.; Namatame, H.; Fujimori, A. *Phys. Rev. B* **1992**, *46*, 3771−3784.
(23) Bocquet, A. E.; Fujimori, A.; Mizokawa, T.; Saitoh, T.; Namatame, H.; Suga, S.; Kimizuka, N.; Takeda, Y.; Takano, M. *Phys. Rev. B* **1992**, *45*, 1561−1570.
(24) Mizokawa, T.; Fujimori, A.; Namatame, H.; Takeda, Y.; Takano, M. *Phys. Rev. B* **1998**, *57*, 9550−9556.
(25) Etani, H.; Yamada, I.; Ohgushi, K.; Hayashi, N.; Kusano, Y.; Mizumaki, M.; Kim, J.; Tsuji, N.; Takahashi, R.; Nishiyama, N.; Inoue, T.; Irifune, T.; Takano, M. *J. Am. Chem. Soc.* **2013**, *135*, 6100−6106.
(26) Izumi, F.; Momma, K. *Solid State Phenom.* **2007**, *130*, 15−20.
(27) Ueda, S.; Katsuya, Y.; Tanaka, M.; Yoshikawa, H.; Yamashita, Y.; Ishimaru, S.; Matsushita, Y.; Kobayashi, K. *AIP Conf. Proc.* **2010**, *1234*, 403.
(28) Ueda, S. *J. Electron Spectrosc. Relat. Phenom.* **2013**, *190*, 235−241.
(29) Kosugi, N.; Kondoh, H.; Tajima, H.; Kuroda, H. *Chem. Phys.* **1989**, *135*, 149−160.
(30) DuBois, J. L.; Mukherjee, P.; Stack, T. D. P.; Hedman, B.; Solomon, E. I.; Hodgson, K. O. *J. Am. Chem. Soc.* **2000**, *122*, 5775−5787.
(31) Mizokawa, T.; Konishi, T.; Fujimori, A.; Hiroi, Z.; Takano, M.; Takeda, Y. *J. Electron Spectrosc. Relat. Phenom.* **1998**, *92*, 97−101.
(32) McGuinness, C.; Downes, J. E.; Sheridan, P.; Glans, P. A.; Smith, K. E.; Si, W.; Johnson, P. D. *Phys. Rev. B* **2005**, *71*, 195111.
(33) Shiraki, H.; Saito, T.; Azuma, M.; Shimakawa, Y. *J. Phys. Soc. Jpn.* **2008**, *77*, 064705.
(34) Morita, Y.; Sudayama, T.; Takubo, K.; Shiraki, H.; Saito, T.; Shimakawa, Y.; Mizokawa, T. *Phys. Rev. B* **2010**, *81*, 165111.
(35) Mizumaki, M.; Mizokawa, T.; Agui, A.; Tanaka, S.; Takatsu, H.; Yonezawa, S.; Maeno, Y. *J. Phys. Soc. Jpn.* **2013**, *82*, 024709.